CERN-ATS-Note-2011-076 TECH

EDMS no: 1160529

September 9, 2011

christian.scheuerlein@cern.ch

A&T Sector Note

Nb_3Sn nucleation and growth in multifilament superconducting strands monitored by high resolution synchrotron diffraction during in-situ reaction

L. Thilly
Institut Pprime, CNRS-University of Poitiers-ENSMA, SP2MI, 86962 Futuroscope, France

M. Di Michiel
European Synchrotron Radiation Facility (ESRF), 38000 Grenoble, France

C. Scheuerlein, B. Bordini
European Organization for Nuclear Research (CERN), CH-1211 Geneva 23, Switzerland

The Nb_3Sn volume, crystallite size and Sn content evolution during the reaction of a recent high critical current density Nb_3Sn/Cu composite wire has been monitored by high energy, high resolution synchrotron x-ray diffraction. Thanks to the high flux of high energy x-rays at the ID15A beamline of the European Synchrotron Radiation Facility it was possible to monitor the Nb_3Sn crystallite growth in-situ from the early stages of Nb_3Sn nucleation at 540 °C, up to nearly complete transformation of the Nb precursor into Nb_3Sn. Simultaneously, the uptake of Sn in the A15 phase could be monitored by Nb_3Sn lattice parameter measurements.

Nb_3Sn strands of the Internal Tin, Powder in Tube and Tube Type design are presently developed and tested for the next generation of superconducting high field magnets, for instance for the Large Hadron Collider (LHC) luminosity upgrade at CERN [1]. Suitable strands must provide a very high critical current density (J_c) at the operating magnetic field and temperature. Today's state-of-the-art Nb_3Sn strands are not optimized: improvements in J_c may come for instance from an increased flux pinning force and a higher and more homogeneously distributed Sn content [2]. It is generally assumed that the main flux pinning centres in Nb_3Sn superconductors are grain boundaries. The optimum flux pinning centre spacing in the A15 phase at 15 T is ~10-20 nm [3]. Since the grain size achieved in modern Nb_3Sn strands varies typically between 120 and 200 nm, substantial improvements in J_c particularly at relatively low field are expected by further decreasing Nb_3Sn grain size. The Sn content in the Nb_3Sn has a strong influence on the upper critical field (B_{c2}) and, therefore, increasing the Sn content is particularly beneficial when the superconductor is operated at high field.

The present study aims at gaining better insight into the Nb_3Sn grain growth and Sn uptake during the reaction of modern multifilament superconductors. Modifications of the Nb-Ta precursor and the Cu matrix during the strand reaction are studied as well, since they influence the Nb_3Sn strain state in the fully reacted composite wire. In addition Nb-Ta grain and sub-grain boundaries may act as Nb_3Sn nucleation sites and, therefore, might influence the size in which Nb_3Sn grains nucleate.

The studied sample is a high-J_c Nb_3Sn strand fabricated by the Restacked Rod Process (RRP) [4] by Oxford Superconducting Technology (OI-ST) (billet #7419). The strand with a nominal diameter of 0.8 mm contains 54 Nb-Ta alloy filament bundles, each surrounded by distributed diffusion barriers. The strand has an effective filament diameter of about 80 µm and it can reach non-Cu critical current density values close to 3000 Amm^{-2} at 12 T, 4.2 K, while maintaining a high purity Cu stabiliser with a RRR of well above 200 [5].

High energy synchrotron x-ray diffraction is an excellent tool for the study of the phase sequence during the Nb_3Sn strand reaction, and its influence on the Nb_3Sn microstructure in the fully reacted strand [6,7,8].

In order to monitor the crystallite growth from the Nb_3Sn diffraction peak width evolution, fast data collection and optimum angular resolution are simultaneously needed. The reported x-ray diffraction experiments have been performed at the ID15A High Energy Scattering beamline of European Synchrotron Radiation Facility (ESRF) in transmission geometry. Debye-Scherrer diffraction patterns were acquired with a high efficiency-high readout speed area detector (Trixell Pixium 4700) with a pixel size of 154 µm. The detector has been placed at a distance of 4899 mm from the sample, in order to have the necessary resolution, while covering a sufficient d-spacing range of 1.3 to 2.8 Å. The detector records only the reflections in the wire drawing axis (x-rays scattering on planes perpendicular to the wire axis). The x-ray energy was 81.435 keV. In order to obtain the required resolution, the x-ray beam has an energy bandwith of ~25 eV. Aluminium compound

Accepted for publication in Applied Physics Letters

refractive lenses, placed just before the sample, focus the beam to the detector, maintaining a high flux and a small spot size on the detector. Instrumental peak broadening has been determined with a LaB_6 reference powder, enabling its deconvolution from experimental spectra using the TOPAS software. The diffraction study is complemented by critical current measurements of an identical wire after isothermal HT of different durations.

The in-situ HT has been performed in a dedicated furnace with temperature accuracy better than ±10 °C. The standard HT performed at CERN is described in [5]. In the synchrotron a HT constituted with heating ramps at 100 °C/h sequentially up to 700 °C, 800 °C and 900 °C, each ramp being followed by a plateau of 4 h (at 700 °C) or 1 h (at 800 °C and 900 °C). Usually, HT temperatures exceeding 700 °C are avoided during the Nb_3Sn reaction. The 1 h-800 °C and 1 h-900 °C plateaus have been added here to explore the full strand reaction and to determine the influence of HT temperature on the Nb_3Sn grain growth. The commonly applied intermediate plateaus at 210 °C and 410 °C have been omitted, which causes a J_c reduction of about 10 % [5]. Diffractograms have been acquired every 5 minutes, i.e. every 8 °C during heating ramps.

Apart from instrumental reasons, diffraction peak broadening occurs mainly because of finite crystallite size effects and non-uniform strain effects. Prior to peak profile analysis, diffractograms were normalised to the x-ray flux reaching the sample, in order to correct for fluctuations of the synchrotron beam current during the experiment.

During HT, several Nb_3Sn peaks appear upon the formation of this phase: only the (200), (210), (320) and (321) reflections could be studied (the (211) reflection being positioned very close to reflections related to intermediate phases that are not studied in this work). All the Cu and Nb_3Sn reflections were fitted with symmetric Pearson VII (PVII) functions. The Nb (110) reflection recorded at RT before HT exhibit a strongly asymmetric profile that is a footprint of a broad distribution of inter-granular stresses in the Nb, associated to the so-called "curling phenomenon" appearing in cold drawn body centred cubic structures [9]: the evolution of this asymmetry will not be studied here but the Nb peak has been fitted using both symmetric and asymmetric functions to check for the validity of the results.

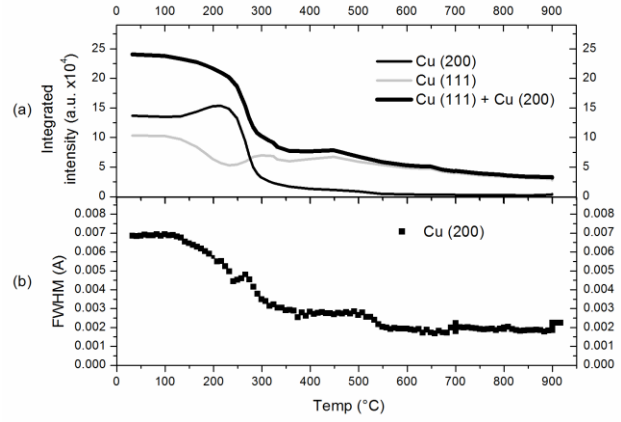

Fig. 1. Evolution of Cu peak characteristics with temperature: (a) Cu (200) and Cu (111) integrated intensity (b) Cu (200) Full Width at Half Maximum (FWHM).

Fig. 1 presents the evolution with temperature of the Cu (200) reflection, i.e. integrated peak intensity (Fig. 1a,) and FWHM (Fig. 1b with inset on peak position). Up to 240 °C, we observe a decrease of FWHM. This regime corresponds to the onset of recovery in the Cu matrix, characterized by a decrease of the <111> texture to the profit of the <200> texture and a reduction of micro-strains stored during the material processing involving cold drawing [9]. Above 240 °C, the peak integrated intensity decreases dramatically, bearing witness for the transformation of Cu into various Cu-Sn intermetallics via Sn diffusion, partly in the liquid state [8]. The remaining Cu undergoes complete recrystallization and grain growth, as shown by the continuous decrease of FWHM.

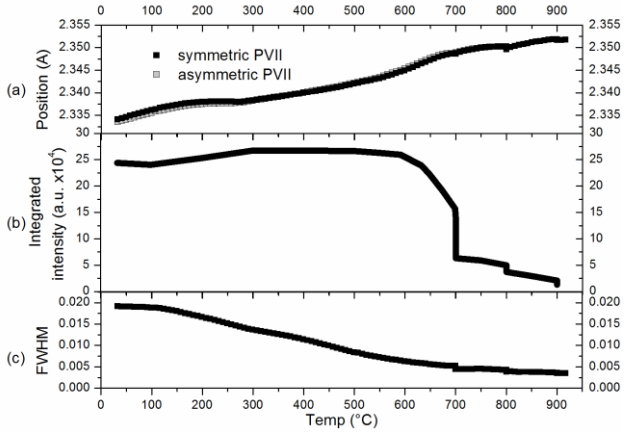

Fig. 2. Evolution of peak characteristics of the Nb (110) reflection with temperature: (a) peak position (results from fit with symmetric PVII or asymmetric PVII functions); (b) peak integrated intensity; (c) peak FWHM.

Fig. 2a presents the evolution of the Nb (110) peak position as a function of temperature for symmetric and asymmetric fits: the difference between the two data sets is less than 0.001 Å at RT and becomes negligible upon HT suggesting that the inter-granular stresses are progressively annealed in the Nb. Therefore, in the following, only the results from symmetric fitting will be discussed for the Nb. In the temperature interval RT to 150 °C, the Nb d-spacing increases linearly with a slope of $\approx 1.23\ 10^{-5}$/K, greater than the coefficient of linear thermal expansion of Nb, $\alpha_{Nb} \approx 0.7\ 10^{-5}$/K [10], as a composite effect with the other phases in the material ($\alpha_{Cu} \approx 1.7\ 10^{-5}$/K). Above 150 °C, the deviation from linear increase indicates the onset of residual stresses relaxation in the Nb filaments, due to Cu softening in their vicinity. Up to 550 °C, the continuous increase of peak height and decrease of peak width is associated to a nearly constant integrated intensity, i.e. a constant diffracting volume for the Nb (Fig. 2b). Only the peak profile is modified (Fig. 2c), as a footprint of the reduction of the distribution of inter-granular stresses in the Nb by recovery processes [9]. Above 600 °C, the integrated intensity decreases strongly, showing a reduction of the Nb volume fraction when Nb and Sn react. At 650 °C and 700 °C, the Nb (110) integrated intensity is reduced by about 17% and 41%, respectively. After the 4 h-700 °C HT the Nb (110) integrated intensity is reduced by about 76 % indicating that most of the Nb has been transformed into Nb_3Sn.

In the RRP strand the Nb_3Sn (200) peak is first detected at 540 °C, at significantly lower temperature than the (320), (321) and (210) peaks [11], and the Nb_3Sn (200) peak remains the largest reflection throughout the entire HT. Therefore, the Nb_3Sn (200) peak has been selected for peak profile analysis. Assuming that the Nb_3Sn grains nucleate and grow in a nearly strain-free state, the decrease of peak width is associated to the increase of grain size. The use of the Scherrer formula allows for a rough calculation of the mean crystallite size of the Nb_3Sn phase. Fig. 3(a) presents the crystallite size evolution after deconvolution of the Nb_3Sn (200) peak from the instrument function.

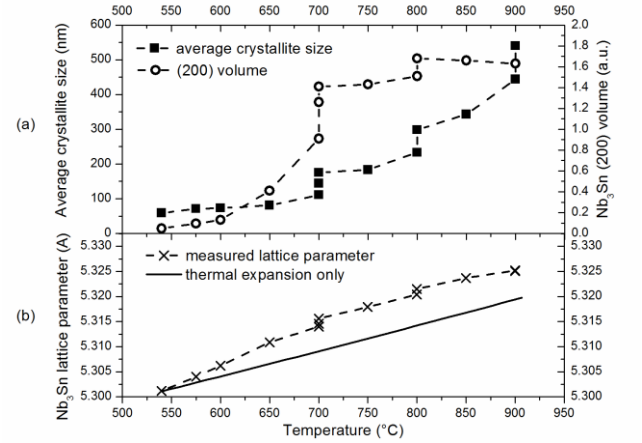

Fig. 3: (a) Average Nb_3Sn crystallite size and volume from Nb_3Sn (200) reflection and (b) Nb_3Sn lattice parameter as a function of temperature. The relative lattice parameter variation induced solely by thermal expansion in the temperature interval 540-900 °C is shown for comparison (see Ref 10).

At 540 °C, i.e. at the onset of detectability, the mean crystallite size is 59 nm, a value that is multiplied by 1.9 at 700 °C (111 nm). After 4 h isothermal heating at 700 °C the Nb_3Sn crystallite size further increases to 175 nm, while the Nb_3Sn volume increases by about 35 %. Further increase in temperature and HT duration only slightly increases the Nb_3Sn volume but has a strong influence on the Nb_3Sn crystallite size, which results in limited J_c at low field, when flux pinning has a dominating influence.

In Fig. 3(b) the Nb_3Sn lattice parameter variation during the in-situ HT is compared with that caused solely by thermal expansion. The relatively strong increase of the lattice parameter in particular at the onset of $Nb_{1-\beta}Sn_\beta$ formation is explained by an increased Sn concentration, which can vary between about 18-25 at.% Sn. For comparison at room temperature the Nb_3Sn lattice parameter increases linearly with increasing Sn content from about 5.28 to 5.29 Å [12]. During 4 h isothermal HT at 700 °C the Nb_3Sn lattice parameter increases from 5.3140 Å to 5.3156 Å, indicating that the average Sn content increases by more than 1%, which in turn corresponds to a B_{c20} increase of 5 T [13]. At high magnetic field such a strong B_{c2} increase outweighs a reduction of flux pinning force due to the simultaneous Nb_3Sn grains growth.

The variation of B_{c2} and the pinning force (C_0) with isothermal 695 °C HT duration has been studied by J_c measurements at 4.3 K and at applied field ranging from 12 T to 9 T with steps of 1 T. The samples were reacted on ITER VAMAS barrels with the duration of the 695 °C plateau ranging from 4-100 hours.

Besides the sample treated for 4 hours, that had a J_c equal to 2600 A/mm^2 at 4.3 K and 12 T, all the other samples (reacted more than 10 hrs at 695 C) had a similar J_c (2910 – 3060 A/mm^2). The relatively lower J_c after only 4 h-HT is explained by the lower Nb_3Sn volume. The diffraction peak evolution shows that the amount of Nb_3Sn formed after 4 h is 87% of that one observed after 1 h at 800 C, which can be considered as the maximum possible for this strand.

In the probed field range, the J_c field dependence can be scaled with the following law: $J_c(B_p,4.3\ K)=C_0\, b^{-0.5}(1-b)^2$ where B_p is the peak field perpendicular to the strand, $b=B_p/\ B_{c2}^*(4.3\ K)$ and B_{c2}^* is the Kramer upper critical field. Using this scaling law and the critical current measurements B_{c2}^* and C_0 have been calculated (Fig. 4). By increasing the HT length B_{c2}^* increases due to the increase of the Sn content in the Nb_3Sn crystals, while the simultaneous C_0 decrease is explained by Nb_3Sn grain growth. The B_{c2}^* value mostly affects the critical current at high fields while the C_0 has a comparatively stronger influence at low field.

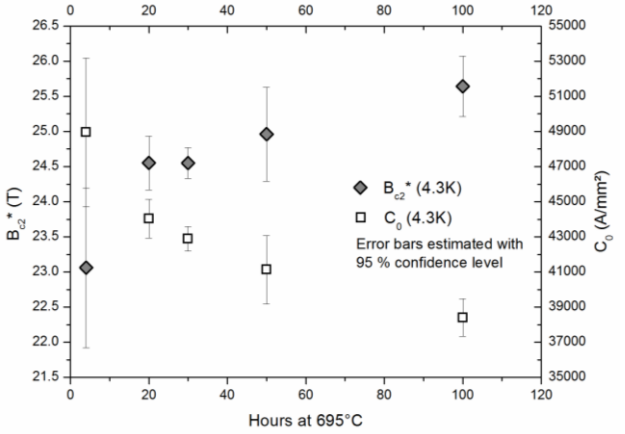

Fig. 4: Evolution of B_{c2} and C_0 as a function of isothermal 695 °C HT duration. For the 4 h-heated sample J_c has been normalised to the Nb_3Sn volume, i.e. J_c*=2600 A mm^{-2} / 0.87).

In summary, high resolution diffraction measurements have allowed to monitor the Nb_3Sn crystallite growth and Sn uptake as a function of HT duration and temperature. Diffraction results are in agreement with J_c results obtained for the same wire, showing how B_{c2} increases and C_0 decreases with HT duration. The data presented allows optimizing the reaction temperature and duration to obtain the best compromise between upper critical field and pinning force at the operating field.

We acknowledge the ESRF for beam time on ID15. We also acknowledge MPI-Stuttgart and H. Reichert for the use of the x-ray Compound Refractive Lenses.

1 G. Ambrosio et al., IEEE Trans. Appl. Supercond. **20**, 283 (2010)
2 P.J. Lee, D.C. Larbalestier, Cryogenics **48**, 283 (2008)
3 A. Godeke, A. den Ouden, A. Nijhuis, H.H.J ten Kate, Cryogenics **48**, 308 (2008)
4 J. A. Parrell, Y. Zhang, M.B. Field, P. Cisek, S. Hong, IEEE Trans. Appl. Supercon. **13**(2), 3470 (2003)
5 B. Bordini, R. Maccaferri, L. Rossi, D. Tommasini, CERN AT-MCS Internal Note 2008-02, EDMS Nr: 907758
6 C. Scheuerlein, M. Di Michiel, A. Haibel, Appl. Phys. Lett. **90**, 132510 (2007)

7 M. Di Michiel, C. Scheuerlein, Supercond. Sci. Technol. **20**, L55-L58 (2007)
8 C. Scheuerlein, M. Di Michiel, G. Arnau, F. Buta, IEEE Trans. Appl. Supercond. **18**(4), 1754 (2008)
9 J.B. Dubois L. Thilly, P.O. Renault, F. Lecouturier, M. Di Michiel, Acta Materialia **58**, 6504 (2010)
10 N. Mitchell, Cryogenics **45**, 501 (2005)
11 C. Scheuerlein, M. Di Michiel, L. Thilly, F. Buta, X. Peng, E. Gregory, J.A. Parrell, I. Pong, B. Bordini, M. Cantoni, J. Phys.: Conf. Ser. 234 022032 (2010)
12 H. Devantay, J.L. Jorda, M. Decroux, J. Müller, R. Flükiger, J. Mat. Sci. **16**, 2145 (1981)
13 R. Flükiger, D. Uglietti, C. Senatore, F. Buta, Cryogenics **48**, 293 (2008)